J Low Temp Phys (2017) 186:285–293
DOI 10.1007/s10909-016-1703-9

Effect of Hafnium Impurities on the Magnetoresistance of $YBa_2Cu_3O_{7-\delta}$

S. V. Savich[1] · A. V. Samoylov[1] · S. N. Kamchatnaya[1] · I. L. Goulatis[1] · R. V. Vovk[1] · A. Chroneos[2,3] · A. L. Solovjov[4] · L. V. Omelchenko[4]

Received: 28 September 2016 / Accepted: 3 November 2016 / Published online: 21 November 2016

Abstract In the present study, we investigate the influence of the hafnium (Hf) impurities on the magnetoresistance of $YBa_2Cu_3O_{7-\delta}$ ceramic samples in the temperature interval of the transition to the superconducting state in constant magnetic field up to 12 T. The cause of the appearance of low- temperature "tails" (paracoherent transitions) on the resistive transitions, corresponding to different phase regimes of the vortex matter state is discussed. At temperatures higher than the critical temperature ($T > T_c$), the temperature dependence of the excess paraconductivity can be described within the Aslamazov–Larkin theoretical model of the fluctuation conductivity for layered superconductors.

Keywords Excess conductivity · $YBa_2Cu_3O_{7-\delta}$ ceramic · Hf impurities · Pinning · 2D–3D crossover · Coherent length

1 Introduction

The discovery of high-temperature superconductivity (HTSC) [1] has created a lot of expectation associated with the possibility of using these materials at temperatures above liquid nitrogen temperatures, in particular, to obtain high magnetic fields.

✉ A. Chroneos
alexander.chroneos@imperial.ac.uk

1 V.N. Karazin Kharkiv National University, Svobody Sq. 4, Kharkiv 61077, Ukraine

2 Department of Materials, Imperial College London, London SW7 2AZ, UK

3 Faculty of Engineering, Environment and Computing, Coventry University, Priory Street, Coventry CV1 5FB, UK

4 B.I. Verkin Institute for Low Temperature Physics and Engineering of National Academy of Science of Ukraine, 47 Nauki Ave., Kharkiv 61103, Ukraine

Nevertheless, the low coherence length [2–4], the large penetration depth [5,6], in conjunction with the presence of intense thermal fluctuations result in thermally activated creep in HTSC observed even at temperatures significantly below the critical ($T << T_c$) [7,8]. Furthermore, the processes in the vortex depinning subsystem is passing much more intensely [5] as compared to classic low-temperature superconductors. As a result, the latter are still unchallenged regarding their application to obtain high magnetic fields. Concurrently, in recent years there is significant progress in improving the critical current density in various types of HTSC compounds, mainly due to the optimization of the composition and the morphology of the defect ensemble [5,9–15].

In the present study, the impact of Hf impurities on the magnetoresistance in $YBa_2Cu_3O_{7-\delta}$ ceramic samples, is investigated. This is a technologically important issue as $YBa_2Cu_3O_{7-\delta}$ is relatively simple to synthesize and has a high critical temperature that exceeds the liquid nitrogen temperature [16–18]. Secondly, this compound has one of the highest—among the HTSC materials—critical currents [5,9]. Thirdly, the presence of intergrain boundaries hinder the diffusion processes of the labile components, contributing to the stability of the oxygen subsystem during long-term operation and aging [17,19,20]. Finally, the introduction of Hf and Zr impurities leads to substitutional impurities, which contribute to the formation of additional pinning centers. These (due to the low coherence length in this HTSC) may also be sufficiently effective on point defects, including oxygen vacancies [21,22] and impurities [5,23]. Here, we investigate the influence of Hf impurities on the magnetoresistive characteristics of $YBa_2Cu_3O_{7-\delta}$ ceramics in the transition interval to the superconducting state.

2 Experimental Methodology

The $YBa_2Cu_3O_{7-\delta}$ ceramic samples were synthesized by the reaction of Y_2O_3, $BaCO_3$, CuO compounds in the temperature interval 750–900°C, in appropriate molar ratios. The resulting powder was pressed under a pressure of 4000 kg/cm^2 in disks (size 20×4 mm) and was sintered at temperatures 950–970°C for 5 h followed by cooling until the room temperature, with intermediate exposures of 2–3 h at temperatures 890 and 530°C. The resulting tablets were superconducting ceramics with rhombic lattice symmetry and $T_c \sim 90$ K. To obtain samples with Hf, we added different amounts of weight concentration (%) of Hf_2O_3. The production and oxygen saturation modes were the same as for the undoped ceramics.

The X-ray diffraction study of the structure and the phase composition of $YBa_2Cu_3O_{7-\delta}$ ceramics in dependence of Hf additives was carried out on the X-ray diffractometer DRON-3 with Cu-K_α-filtered radiation. The profiles of X-ray diffraction maxima were produced by scanning in manual mode (angles' intervals $2\theta = 0.1°$ in the background and through $2\theta = 0.02°$ at maximum). Analysis of the radiographs showed that the initial sample has an orthorhombic perovskite crystal structure with lattice parameters: $a = 3.8348$Å, $b = 3.8895$Å, $c = 11.6790$Å, which is consistent to previous studies. By increasing the content of hafnium oxide additives (Hf_2O_3), the intensity of X-ray diffraction peaks corresponding to the original structure is reduced, and in the radiographs X-ray diffraction peaks appear that correspond to

the orthorhombic perovskite structure (but with larger lattice parameters). As a result of our measurements, it was established that increasing the content of Hf the phase composition of the samples changes. The amount of the initial orthorhombic phase decreases and the proportion of the orthorhombic phase with increased lattice parameter increases.

The electrical contacts are created on a standard four-contact scheme by depositing indium on the surface of the sample, followed by connecting the 0.05-mm-diameter silver wires. The measurements were performed in the drift mode at two opposite directions of transport current to eliminate the influence of interference signal. The temperature was measured by a platinum thermistor, and the voltage by V2-38 nanovoltmeters. The critical temperature was determined at the maximum point on the curves $d\rho_{ab}(T)/dT$ in the superconducting transition interval. The magnetic field of 12 T was produced by a superconducting solenoid.

3 Results and Discussion

To investigate the resistive transition to the superconducting state (SCS), we used the Kouvel–Fisher method [24], which is based on the analysis of the value $\chi = \frac{-d(\ln \Delta\sigma)}{dT}$, where $\Delta\sigma = \sigma - \sigma_0$ is an amendment to the conductivity occurring in the conductive subsystem due to fluctuation pairing carriers at $T > T_c$ [25,26] and determined by the phase state of the vortex matter at $T < T_c$ [27,28]. Here, $\sigma = \rho^{-1}$ is the experimentally measured conductivity value, and $\sigma_0 = \rho_0^{-1} = (A+BT)^{-1}$ is the regularly subtracted term determined by extrapolating the linear high-temperature portion until the region of the SCS transition. Assuming that $\Delta\sigma$ diverges as $\Delta\sigma \sim (T - T_c)^{-\beta}$ at $T \approx T_c$, from the derivative $\chi = \frac{-d(\ln \Delta\sigma)}{dT}$ follows that $\chi^{-1} = \beta^{-1}(T - T_c)$, where β is an index that depends on the dimension and the phase state of the fluctuation and vortex subsystems [23,25–28]. Thus, the identification of linear temperature areas on the $\chi^{-1}(T)$ dependence allows the simultaneous determination of critical dimension indexes and the characteristic temperatures of the dynamic-phase transitions in the subsystem of the superconducting carriers.

Fig. 1 shows the temperature dependence of the resistivity in the basal ab-plane $\rho_{ab}(T)$, measured at H=0. The inset shows the resistive transition to the superconducting state at different magnetic fields ranging from H = 0–12 T. As it can be observed, when the temperature is lowered below 300 K, the $\rho(T)$ decreases almost linearly down to a characteristic temperature $T^* \approx 141$ K. Below this temperature begins a systematic downward deviation of the experimental points from the linear dependence indicating the appearance of excess conductivity $\Delta\sigma$, as it was mentioned above. This behavior in $\rho_{ab}(T)$ dependence at temperatures $T >> T_c$ is due to the manifestation of the "pseudogap anomalies" (PG) (refer to [17]). Notably, the application of the magnetic field, within the experimental error limits, is not affecting the behavior of the curves $\rho(T)$ above the SCS transition and results in a significant broadening of the superconducting transition, in comparison with the sufficiently sharp ($\Delta T_c \approx 1.5$ K) transition, that was observed at $H = 0$.

There is a significant difference in the form of the resistive transitions to the superconducting state, between those that are usually observed in the magnetic field for the

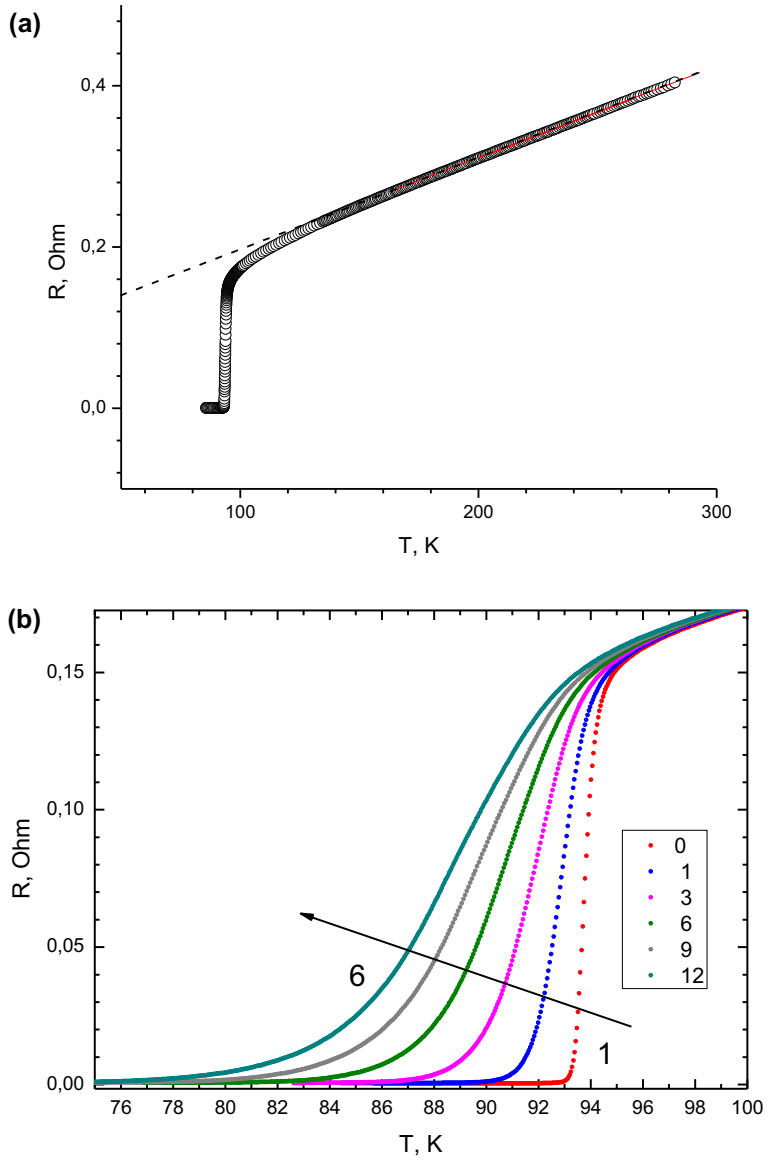

Fig. 1 Temperature dependence of the resistivity R of $YBa_2Cu_3O_{7-\delta}$ with Hf impurities (**a**) for $H = 0$, 1, 3, 6, 9, 12 T—curves 1–6, respectively (**b**). The *dotted lines* represent the extrapolation of the linear portion in the region of low temperatures (Color figure online)

undoped samples [7,29] and those of the present sample that contains Hf impurities. In the first case on the tail of the superconducting transition, a sharp "kink" is usually observed and this is a monotonic smoothing of the low-temperature portion of the resistive transition. The latter is reflected in the actual disappearance of the low-temperature peak in the temperature dependences of the derivative $d\rho_{ab}(T)/dT$ (refer

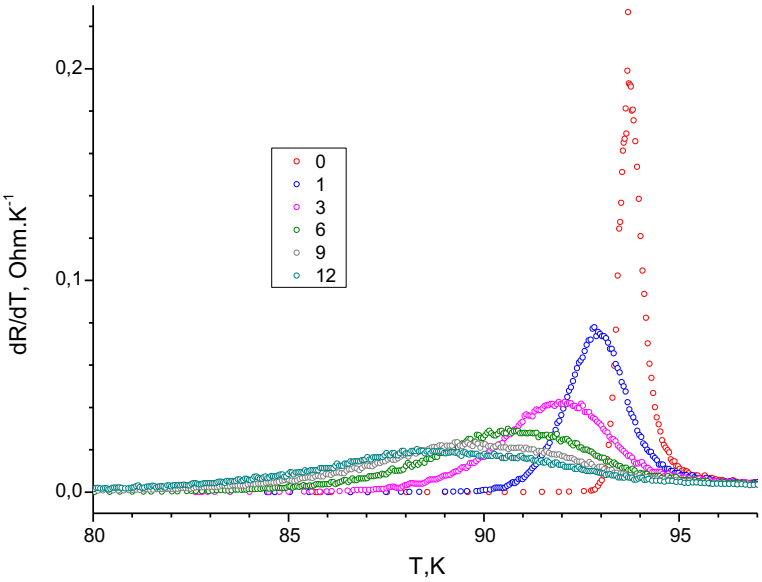

Fig. 2 Resistive transition to the superconducting state for the $YBa_2Cu_3O_{7-\delta}$+ 37.5% Hf_2O_3 in dR/dT versus T coordinates. The numbering of the curves is consistent to Fig. 1 (Color figure online)

to Fig. 2). As it was previously determined [19,23], the appearance of such features in the temperature dependences $\rho_{ab}(T)$ and d$\rho_{ab}(T)$/dT testifies the implementation in the system of a first-order phase transition corresponding to the melting of the vortex lattice. The disappearance of these features in the case of Hf-doped $YBa_2Cu_3O_{7-\delta}$ can indicate the suppression of such a transition. At the same time, we should consider that in this case the resistive transitions exhibit some universal dependence, running over the slope located on the left from the main high-temperature peak of the d$\rho_{ab}(T)$/dT dependence. According to previous studies [27], the temperature corresponding to this peak is the critical temperature in the mean-field approximation T_c^{mf}. This, in turn, can indicate the realization in the system of a new state in the conductive subsystem.

Fig. 3 shows the resistive transition to the superconducting state in $\left[\frac{-d(\ln \Delta\sigma)}{dT}\right]^{-1} - T$ coordinates. In the high-temperature SCS transition, in all curves we observed a somewhat extended linear section with a slope angle $\beta \approx 0.5$ that, according to previous work [25], indicates the implementation of a three-dimensional (3D) mode of fluctuation carriers' existence in the system. Herewith, the area corresponding to 3D mode is significantly unstable in a magnetic field, which is consistent with the results obtained by Costa et al. [23]. When increasing the temperature from T_c to higher temperatures, there occurs a further increase in the absolute value of β, which can indicate the realization of a 3D-2D crossover in the system [25,26].

The application of magnetic field leads to a significant broadening and smearing of the SCS transition. It is established [22,29] that this may result by the presence of strong pinning centers in the system, contributing to the blurring of the aforementioned kink and to the transition from the phase of the ordered vortex lattice to the phase, of

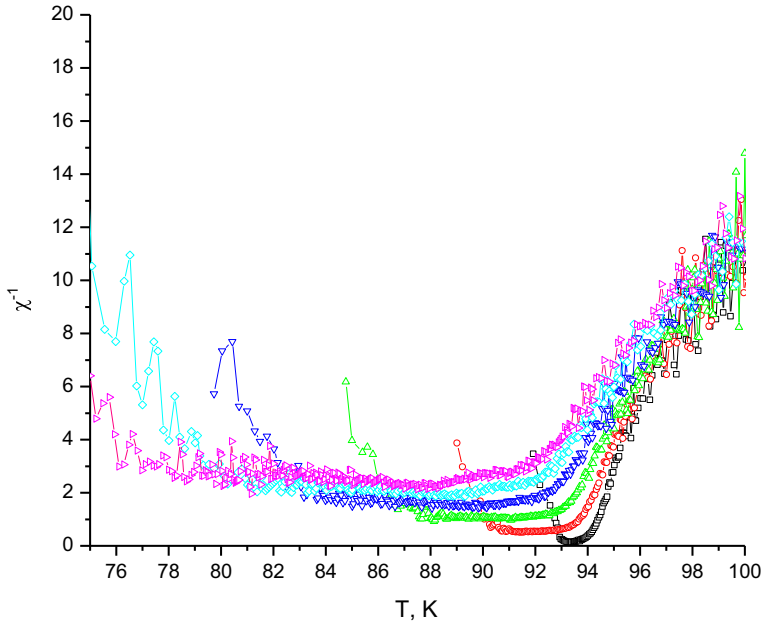

Fig. 3 Resistive transition to the superconducting state for the $YBa_2Cu_3O_{7-\delta}$+ 37.5% Hf_2O_3 in $\left[\frac{-d(\ln \Delta\sigma)}{dT}\right]^{-1} - T$ coordinates. The numbering of the curves is consistent to Fig. 1 (Color figure online)

the so-called "vortex" or "Bragg" glass, which is conditioned by the accommodation of the vortex system to chaotic pinning potential. That is, a chaotic pinning potential violates the long-range order of the vortex lattice, thereby suppressing the first-order phase transition and promoting the implementation of the glassy state of the vortices [22]. At the same time on the resistive transitions appear extended "tails," the amplitude of which is less than the resistance of viscous flow ρ_{ff}, which is probably due to the partial pinning of the vortex liquid.

In the present study, this potential can be due to the intergrain boundaries or the inclusion of a new phase, arising from the introduction of Hf impurities. In favor of the latter assumption is the radiographic study of our samples that registered the presence of such a phase (see above), despite the fact that the effect of "kink smearing" is often not observed in samples 1–2–3 without Hf impurities [5,29], or with impurities, resulting in the total or partial substitution of the initial component [27]. Thus, we can assume that in the sample coexist pinning potential, generated by intergrain boundaries, and volume pinning owing to the order parameter suppression induced by the Hf impurities.

As it was shown by Costa et al. [23], in the case of implementation "Bragg glass" state in the system on the $\chi(T)$ curves there should be scaling in reduced $\chi(T_c\text{-}T_{c0})$ versus $(T - T_{c0})/(T_c - T_{c0})$ coordinates, where T_{c0} is the critical temperature of the end of the transition in the paracoherent area. This is determined in the intersection of the linear section, approximating the so-called paracoherent area with the axis

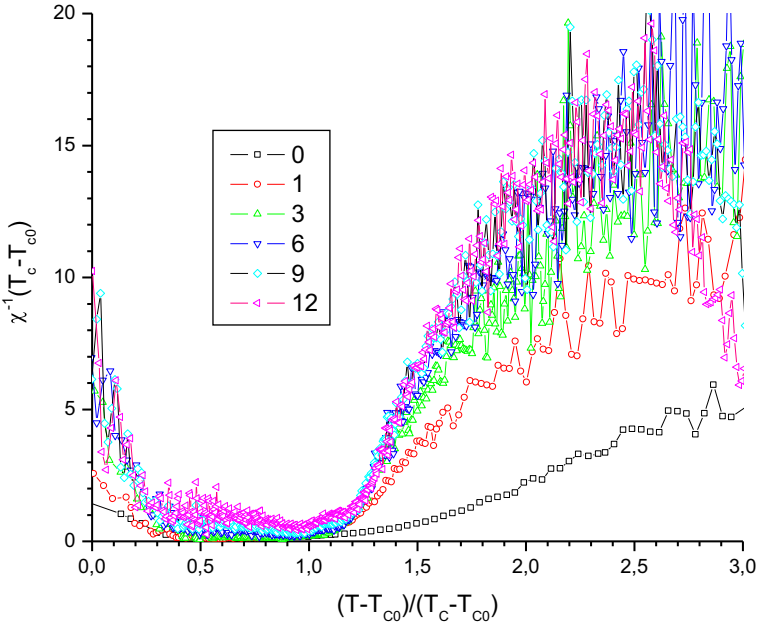

Fig. 4 Resistive transition to the superconducting state for the $YBa_2Cu_3O_{7-\delta}$+ 37.5% Hf_2O_3 in $\chi(T_c - T_{c0})$ versus $(T - T_{c0})/(T_c\text{-}T_{c0})$ coordinates. The numbering of the curves is consistent to Fig. 1 (Color figure online)

of temperature and T_c is the temperature corresponding to the mean-field critical temperature, which is determined at the maximum point on the curves $d\rho_{ab}(T)/dT$.

Fig. 4 shows the same curves, scaled as $\chi(T_c\text{-}T_{c0})$ versus $(T - T_{c0})/(T_c - T_{c0})$. As it can be observed from Fig. 4, on the experimental curves the best scaling is in the paracoherent area at $T < T_c$. At higher temperatures, the spread of the curves becomes significant, apparently, due to the influence of the pinning of the superconducting fluctuations in the phase inclusions, as well as with the possible increase of the role of some specific mechanisms of the quasi-particle interaction [30–34].

4 Conclusions

We can conclude that in the immediate vicinity of T_c the fluctuation conductivity can be described by the 3D Aslamazov–Larkin model for the layered superconducting systems. The application of a constant magnetic field to $YBa_2Cu_3O_{7-\delta}$ samples with Hf impurities, in contrast to similar, undoped samples, leads to a smearing of the additional paracoherent transition to the temperature dependence of the excess conductivity in the basal ab-plane in the area of the resistive transition to the superconducting state. This can be due to the influence of the volume pinning, caused by the presence of phase inclusions in the structure of the experimental sample, formed by the introduction of Hf impurities. As a result, at temperatures below the critical $T < T_c$, there is a

suppression of the dynamic-phase-transition-type liquid vortex–vortex lattice and the formation of a transition-type liquid vortex–vortex "Bragg" glass in the system.

References

1. J.G. Bednorz, K.A. Muller, Z. Phys. B **64**, 189 (1986)
2. T.A. Friedmann, J.P. Rice, J. Giapintzakis, D.M. Ginsberg, Phys. Rev. B **39**, 4258 (1989)
3. R.V. Vovk, G.Ya. Khadzhai, I.L. Goulatis, A. Chroneos, Phys. B **436**, 88 (2014)
4. A. Solovjov, M. Tkachenko, R.V. Vovk, A. Chroneos, Phys. C **501**, 24 (2014)
5. G. Blatter, M.V. Feigel'man, V.B. Geshkenbein, A.I. Larkin, V.M. Vinokur, Rev. Mod. Phys. **66**, 1125 (1994)
6. D.D. Balla, A.V. Bondarenko, R.V. Vovk, M.A. Obolenskii, A.A. Prodan, Low Temp. Phys. **23**, 777 (1997)
7. A.V. Bondarenko, V.A. Shklovskij, R.V. Vovk, M.A. Obolenskii, A.A. Prodan, Low Temp. Phys. **23**, 962 (1997)
8. A.V. Bondarenko, V.A. Shklovskij, M.A. Obolenskii, R.V. Vovk, A.A. Prodan, M. Pissa, D. Niarchos, G. Kallias, Phys. Rev. B **58**, 2445 (1998)
9. V.M. Pan, V.L. Svechnikov, V.F. Solovjov, Supercond. Sci. Technol. **5**, 707 (1992)
10. R.V. Vovk, M.A. Obolenskii, A.A. Zavgorodniy, Z.F. Nazyrov, I.L. Goulatis, V.V. Kruglyak, A. Chroneos, Mod. Phys. Lett. B **25**, 2131 (2011)
11. R.V. Vovk, M.A. Obolenskii, A.A. Zavgorodniy, A.V. Bondarenko, I.L. Goulatis, A.V. Samoilov, A. Chroneos, J. Alloys Compd. **453**, 69 (2008)
12. R.V. Vovk, M.A. Obolenskii, A.A. Zavgorodniy, I.L. Goulatis, V.I. Beletskii, A. Chroneos, Phys. C **469**, 203 (2009)
13. R.V. Vovk, Z.F. Nazyrov, M.A. Obolenskii, I.L. Goulatis, A. Chroneos, V.M.P. Simoes, Philos. Mag. **91**, 2291 (2011)
14. R.V. Vovk, M.A. Obolenskii, Z.F. Nazyrov, I.L. Goulatis, A. Chroneos, V.M.P. Simoes, J. Mater. Sci. Mater. Electron. **23**, 1255 (2012)
15. R.V. Vovk, N.R. Vovk, O.V. Shekhovtsov, I.L. Goulatis, A. Chroneos, Supercond. Sci. Technol. **26**, 085017 (2013)
16. Z. Li, H. Wang, N. Yang, X. Jin, L. Shen, J. Chin. Ceram. Soc. **18**, 555 (1990)
17. S.V. Savich, A.V. Samoilov, R.V. Vovk, O.V. Dobrovolskiyl, S.N. Kamchatna, Ya V. Dolgopolova, O.A. Chernovol-Tkachenko, Mod. Phys. Lett. B **30**, 1650034 (2016)
18. M.K. Wu, J.R. Ashburn, C.J. Torng, P.H. Hor, R.L. Meng, L. Gao, Z.J. Huang, Y.Q. Wang, C.W. Chu, Phys. Rev. Lett. **58**, 908 (1987)
19. B. Martinez, F. Sandiumenge, S. Pinol, N. Vilalta, J. Fontcuberta, X. Obradors, Appl. Phys. Lett. **66**, 772 (1995)
20. R.V. Vovk, N.R. Vovk, A.V. Samoilov, I.L. Goulatis, A. Chroneos, Solid State Commun. **170**, 6 (2013)
21. T. Kemin, H. Meisheng, W. Yening, J. Phys. Condens. Matter **1**, 1049 (1989)
22. R.V. Vovk, Z.F. Nazyrov, M.A. Obolenskii, I.L. Goulatis, A. Chroneos, V.M.P. Simoes, J. Alloys Compd. **509**, 4553 (2011)
23. R.M. Costa, I.C. Riegel, A.R. Jurelo, J.L. Pimentel Jr., J. Magn. Magn. Mater. **320**, E493 (2008)
24. J.S. Kouvel, M.E. Fischer, Phys. Rev. **136**, 1616 (1964)
25. L.G. Aslamazov, A.I. Larkin, Phys. Lett. **26A**, 238 (1968)
26. R.V. Vovk, N.R. Vovk, G.Y. Khadzhai, O.V. Dobrovolskiy, Z.F. Nazyrov, Curr. Appl. Phys. **14**, 1779 (2014)
27. J. Roa-Rojas, R. Menegotto Costa, P. Pureur, Phys. Rev. B **61**, 12457 (2000)
28. R.V. Vovk, V.M. Gvozdikov, M.A. Obolenskii, Z.F. Nazyrov, V.V. Kruglyak, Acta Phys. Pol. A **121**, 1191 (2012)

29. W.K. Kwok, S. Fleshler, U. Welp, V.M. Vinokur, J. Downey, G.W. Crabtree, M.M. Miller, Phys. Rev. Lett. **69**, 3370 (1992)
30. R.V. Vovk, G.Ya. Khadzhai, O.V. Dobrovolskiy, Appl. Phys. A **117**, 997–1002 (2014)
31. V.N. Golovach, M.E. Portnoi, Phys. Rev. B **74**, 085321 (2006)
32. R.V. Vovk, Z.F. Nazyrov, I.L. Goulatis, A. Chroneos, Phys. C **485**, 89 (2013)
33. U. Schwingenschlögl, C. Schuster, Appl. Phys. Lett **100**, 253111 (2012)
34. P.G. Curran, V.V. Khotkevych, S.J. Bending, A.S. Gibbs, S.L. Lee, A.P. Mackenzie, Phys. Rev. B **84**, 104507 (2011)